Growth-mediated autochemotactic pattern formation in self-propelling bacteria

Mrinmoy Mukherjee* and Pushpita Ghosh†
Tata Institute of Fundamental Research, Hyderabad 500107, India

(Received 30 November 2017; published 31 January 2018)

Bacteria, while developing a multicellular colony or biofilm, can undergo pattern formation by diverse intricate mechanisms. One such route is directional movement or chemotaxis toward or away from self-secreted or externally employed chemicals. In some bacteria, the self-produced signaling chemicals or autoinducers themselves act as chemoattractants or chemorepellents and thereby regulate the directional movements of the cells in the colony. In addition, bacteria follow a certain growth kinetics which is integrated in the process of colony development. Here, we study the interplay of bacterial growth dynamics, cell motility, and autochemotactic motion with respect to the self-secreted diffusive signaling chemicals in spatial pattern formation. Using a continuum model of motile bacteria, we show growth can act as a crucial tuning parameter in determining the spatiotemporal dynamics of a colony. In action of growth dynamics, while chemoattraction toward autoinducers creates arrested phase separation, pattern transitions and suppression can occur for a fixed chemorepulsive strength.

DOI: 10.1103/PhysRevE.97.012413

I. INTRODUCTION

Pattern formation through self-aggregation of cells is a common trait in the multicellular microbial community [1–5]. Various biochemical and mechanical processes such as cell growth, death, movement, and secretion of extracellular polymeric substances, contribute in the process of self-organization [6–10]. In addition, bacteria also secrete signaling molecules or autoinducers for intricate chemical communications among the cells [11,12]. The self-secreted extracellular substances by bacteria can regulate the spatial patterning of a growing colony by directing or trapping the motions of the cells in a growing colony [12–15]. The underlying mechanisms of forming a spatially patterned colony and the spatiotemporal organization of cells inside it, are themselves very complex. Previous studies have explored several mechanisms underlying pattern formation in bacteria such as density-dependent motility [15–18], temporal control of gene expression [19], quorum sensing [11,20,21], and the widely studied phenomenon of chemotaxis [22–27].

The process of chemotaxis involves detection of chemical gradients by the bacterial cells and biasing their self-propulsive direction according to the chemical gradient. Two types of chemotactic mechanisms are possible. Bacteria can swim toward the self-secreted or externally employed chemicals such as food or nutrients [23,28,29], (chemoattraction) or move away from it in the case of antibiotics or toxins [30] (chemorepulsion). The formation of different patterns such as spots, stripes, concentric rings and waves, etc., in the colonies of *Escherichia coli* or *Salmonella typhimurium* stems from chemotactic drift motion of the microbial cells [12,31,32]. Chemoattraction is broadly studied in the literature in different contexts [22–27]. The classic model, which can describe chemoattractive instability, is called the Keller-Segel model [22,33]. Recently, Liebchen *et al.* [34,35] have shown the mechanism of clustering and pattern formation in the context of autophoretic active colloids.

As mentioned earlier, many bacterial species can produce and sense extracellular signaling molecules or autoinducers. In shorter time scales, the chemotactic response toward autoinducers helps to form heterogeneous structures during biofilm formation [12,13]. However, the type of chemotactic response is specific to the system. For example, in the case of *Helicobacter pylori*, AI-2 autoinducer acts as a chemorepellant, but for *E. coli*, AI-2 works as a chemoattractant [30]. In addition to the chemotactic response, growth dynamics is an integral and prominent feature of any microbial system. Growth can significantly influence the structure and the type of the emergent spatial orders in bacteria. The time scale of growth kinetics ($\sim$1 h) is generally faster than the time scale of pattern formation ($\sim$1 day) [16] and thus gives an additional feature in governing the spatiotemporal dynamics. In this regard, the questions that still remain to be explored in detail are as follows: (i) What happens when the self-secreted autoinducers by bacteria itself act as chemoattractants or chemorepellants? (ii) How and to what extent can the autochemotaxis coupled with the inherent growth dynamics influence the spatiotemporal organization in an active microbial colony? (iii) To what extent does the orientation of bacterial cells regulate the pattern formation?

The object of the present work is to explore the interplay of bacterial growth kinetics and chemotactic movement with respect to self-secreted chemicals in a colony of motile bacteria. We use a continuum model as described in [34] with an additional term which accounts for the logistic growth of self-propelling bacteria. This kind of model can also be derived from fundamental microscopic quantities as discussed in [35,36]. We focus on the effect of bacterial growth kinetics on the spatiotemporal organization of a colony, for both the cases of chemoattraction and chemorepulsion. In what follows, we show that in the case of chemoattraction, growth can arrest

*mrinmoym@tifrh.res.in
†Corresponding author: pghosh@tifrh.res.in

the continuous aggregation of bacteria locally, resulting in a self-organized pattern of bacterial density of well-defined wavelength. However, in the case of chemorepulsion, growth can tune the parametric region of instability leading to the transitions from oscillatory to stationary patterns either directly or, more interestingly, via an intermediate homogeneous state. Altogether, our results suggest that growth kinetics facilitates the formation of stationary patterns in a developing microbial colony.

The rest of the paper is organized as follows: In Sec. II, we describe the model and method to investigate the spatiotemporal dynamics. Section III demonstrates the results and includes discussions for both cases of autochemotaxis. The paper is concluded in Sec. IV.

II. MODEL AND METHOD

To investigate the spatiotemporal dynamics of a microbial colony, we consider a spatially extended system of three variables: the bacterial density $\rho(\vec{r},t)$, polarization $\vec{p}(\vec{r},t)$, and the self-secreted chemical density $c(\vec{r},t)$ using the model described in [34] with an additional term corresponding to population growth. The reproduction and death of bacteria are modeled by considering a classic logistic growth term in our model. The model is represented by the following equations:

$$\begin{aligned}\dot{\rho} &= -\overrightarrow{\nabla}\cdot(\rho v_0\vec{p}) + \mathcal{D}_\rho\nabla^2\rho + \alpha\rho(1-\rho/K),\\ \dot{\vec{p}} &= -\gamma\vec{p} + \mathcal{D}_p\nabla^2\vec{p} + \beta\overrightarrow{\nabla}c - \gamma_2|\vec{p}^{\,2}|\vec{p},\\ \dot{c} &= \mathcal{D}_c\nabla^2 c + (k_0\rho - k_d c) + k_a\overrightarrow{\nabla}\cdot(\rho\vec{p}),\end{aligned} \tag{1}$$

where v_0 is the self-propulsion speed of the bacteria which behaves as a constant. The time evolution of ρ depends on three terms: drift, diffusion, and logistic growth. Here, $\mathcal{D}_\rho$ represents the diffusion constant, α is the growth rate, and K stands for the carrying capacity of the bacteria. The local average of the propulsive unit vectors per unit volume or polarization ($\vec{p}$) orients according to the gradient of chemical density (c), where β measures the chemotactic strength. If β is positive, bacteria orient themselves toward the chemical gradient which is called chemoattraction. Similarly, negative β represents chemorepulsion. γ is the decay rate of $\vec{p}$ set by rotational diffusion ($1/\gamma$ represents orientational relaxation time) [18] and $\mathcal{D}_p$ is the translational diffusion constant. The last term with the parameter γ_2 in the equation of polarization ensures saturation of polarization at strong alignment [34,37]. The chemical substance is produced from bacteria at a local rate k_0 and naturally degraded at a rate k_d. The term with k_a describes an anisotropic correction to the isotropic secretion term $k_0\rho$, whenever there is any asymmetry in the secretion of signaling chemicals from the microbial cells as discussed in [34,35] for Janus colloids. Although the production and secretion of chemical signaling molecules from bacteria is a complex process and very little is known at a subcellular level, we can assume a point source $-R_0\mathbf{p}$ away from cell center with R_0 as the radius of the cell, then the anisotropic term follows as the lowest order correction to the isotropic field, with $k_a \sim k_0 R_0$. The secreted chemical field diffuses with a diffusion constant $\mathcal{D}_c$. Although our model represents the spatiotemporal dynamics of signaling bacteria, a similar model can be applicable for other signaling microorganisms or active eukaryotic cells which shows chemotactic movements.

TABLE I. Parameters.

Parameter	Ranges (Refs.)	Dimensionless parameters	Simulations
α	$1\,\mathrm{h}^{-1}$ [16]	D_p	1
v_0	10–100 $\mu\mathrm{m\,s}^{-1}$ [23]	D_c	1
$\mathcal{D}_\rho$	(2–4) $\times 10^{-6}$ $\mathrm{cm^2\,s^{-1}}$ [24,25]	Γ	1
$\mathcal{D}_c$	8.9×10^{-6} $\mathrm{cm^2\,s^{-1}}$ [24,25]	k	0–1
$\mathcal{D}_p$	$\approx\mathcal{D}_\rho$ [34]	g	0–5
k_d	10^{-4}–10^{-2} $\mathrm{s^{-1}}$ [23]	Γ_2	10

Rewriting Eqs. (1) in dimensionless form by defining $\rho^* = \rho/K$, $\vec{p}^{\,*} = (v_0/\sqrt{k_d\mathcal{D}_\rho})\vec{p}$, $c^* = (k_d/k_0K)c$, $t^* = k_d t$, and $\vec{r}^{\,*} = \vec{r}\sqrt{k_d/\mathcal{D}_\rho}$, we get the following equations:

$$\begin{aligned}\dot{\rho} &= -\overrightarrow{\nabla}\cdot(\rho\vec{p}) + \nabla^2\rho + g\rho(1-\rho),\\ \dot{\vec{p}} &= -\Gamma\vec{p} + D_p\nabla^2\vec{p} + \chi\overrightarrow{\nabla}c - \Gamma_2|\vec{p}^{\,2}|\vec{p},\\ \dot{c} &= D_c\nabla^2 c + \rho - c + k\overrightarrow{\nabla}\cdot(\rho\vec{p}).\end{aligned} \tag{2}$$

We remove the asterisks from Eqs. (2) for simplicity. Out of the seven dimensionless parameters, $g = \alpha/k_d$, $\Gamma = \gamma/k_d$, $D_p = \mathcal{D}_p/\mathcal{D}_\rho$, $\chi = (\beta k_0 v_0 K)/(k_d^2\mathcal{D}_\rho)$, $\Gamma_2 = \gamma_2\mathcal{D}_\rho/v_0^2$, $D_c = \mathcal{D}_c/\mathcal{D}_\rho$, and $k = (k_a k_d)/(k_0 v_0)$, we will mainly focus on the role of growth rate g, chemotactic strength χ, and anisotropic production rate k. Here, positive χ represents chemoattraction and negative χ represents chemorepulsion.

The values of the above-mentioned parameters depend on the particular bacterial species and external conditions such as the growth medium, food, surface, etc. From the existing literature, we can get the typical range of the values of several of these parameters (see Table I). In our present study, we choose the values of our dimensionless parameters as given in Table I. For the asymmetric production of chemicals, we assume the value of k varies from 0 to 1 (our numerical scheme is not stable for higher values of k, although chemoattraction sets an upper limit of k at fixed g; for details, see the Appendix). We choose $\Gamma = 1$ for most of the cases (a higher value of Γ is allowed since α is relatively lower than γ in bacteria [17]). We allow the chemotactic strength, χ, to vary from 0 to higher values as a free parameter.

The uniform states of the system obtained from Eqs. (2) are $(\rho,\vec{p},c) = (0,\vec{0},0)$ and $(1,\vec{0},1)$. The state $(0,\vec{0},0)$ is always unstable with respect to an infinitesimal small perturbation. By linear stability analysis of the system described by Eqs. (2), we obtain the bifurcation diagrams to find the region of spatial instability. We numerically solve Eqs. (2) by using a simple Euler method for time stepping and a central finite difference scheme to evaluate the spatial derivatives in a square box of size $L = 100$, using a periodic boundary condition (unless otherwise mentioned). The grid length and time step for the simulations are 0.2 and 10^{-3}, respectively. The initial condition we use as a small perturbation of the uniform state $(1,\vec{0},1)$.

III. RESULTS AND DISCUSSION

Our objective here is to understand the interplay of growth rate and chemotactic drift of the cells with respect to the self-secreted signaling chemicals on the spatiotemporal organization of a bacteria colony. Assuming bacteria can produce the signaling molecules both isotropically ($k = 0$) and anisotropically ($k \neq 0$), we investigate how chemoattraction or repulsion gives rise to the spatiotemporal instabilities in bacteria in the presence of logistic growth dynamics. In what follows, we begin our study with positive autochemotaxis.

A. Emergent patterns due to chemoattraction

In the case of chemoattraction ($\chi = s, s > 0$), bacteria propel themselves toward the self-secreted chemicals (signaling molecules) and form aggregates. Due to a positive feedback, as bacteria aggregate, more chemicals are being produced which thereby attract more bacteria. As a result, there occurs a continuous aggregation of bacterial droplets with time as shown in Figs. 1(a) and 1(b) in the absence of any growth dynamics (i.e., $g = 0$). This continuous accumulation of bacteria is not very realistic as bacteria density cannot grow locally without any bound. However, the presence of a logistic growth kinetics in the system arrests the continuous aggregation of bacteria by choosing a characteristic domain size and developing a stationary pattern of bacteria density. There occurs a balance between diffusion, chemotactic drift, and birth-death dynamics. We observe the formation of stationary spot patterns of well-attained steady-state sizes and center-to-center distances as demonstrated in Figs. 1(c) and 1(d) in the presence of logistic growth kinetics, i.e., $g \neq 0$. The corresponding spatiotemporal evolution of patterns is illustrated in videos 1 and 2 in the Supplemental Material [38]. This observation can be further complemented by determining the evolution of the characteristic domain size, $L(t)$, which is computed as the inverse of the first moment of the structure factor [16] (for the details of quantification, see the Appendix). Figure 1(e) shows that $L(t)$ at late time finally reaches to a steady state at a constant value with no further change for the $g \neq 0$ case, whereas, it shows a slow decrease and is still not able to reach any steady-state value in the absence of growth kinetics ($g = 0$). In fact, for the $g = 0$ case, the size of a single droplet in the process of coarsening is almost fixed over time but its concentration is increasing after growing out of the initial uniform state. The other droplets are disappearing with time. Hence, we see a slightly decreasing behavior in $L(t)$. We have also checked that the average area of the droplets shows a decreasing trend with time by calculating the contour area of the droplets (not shown here). This dynamics does not follow the usual behavior of a phase-separating system where coarsening increases the characteristic domain size with time. These results strongly support the necessity of a self-limiting mechanism in growing bacteria by the presence of its growth-death dynamics.

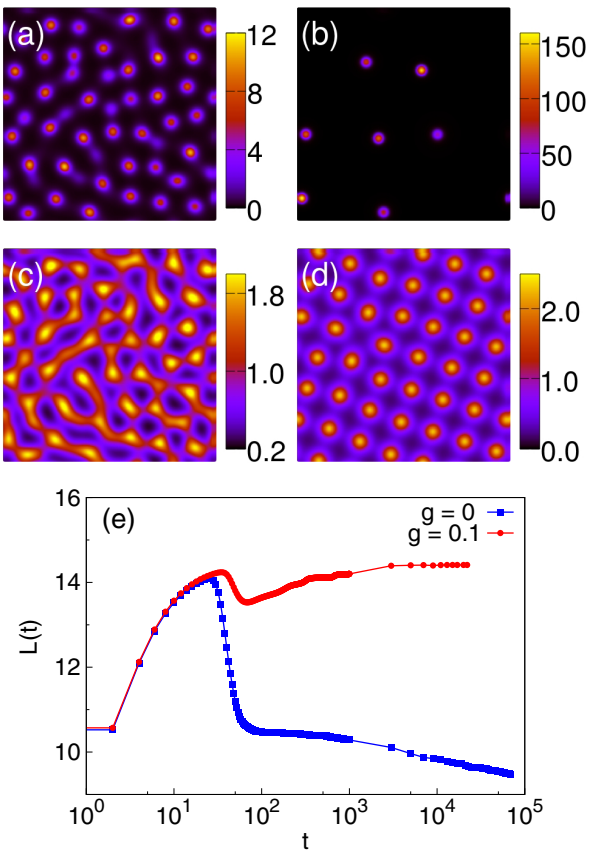

FIG. 1. Snapshots of the density field of bacteria in the case of chemoattraction. Time has increased from (a) to (b) and (c) to (d). In the presence of the logistic growth rate ($g = 0.1$), the phase separation is arrested in (c) and (d). However, it shows a continuous aggregation in the absence of growth rate $g = 0.0$ from (a) to (b) as time evolves for the parameters $s = 10$, $k = 1.0$. (e) Plot of the characteristic domain size of the pattern, quantified by the inverse of the first moment of the structure factor $L(t)$ as a function of time, t (in logarithmic scale). All other parameters are kept the same as given in Table I.

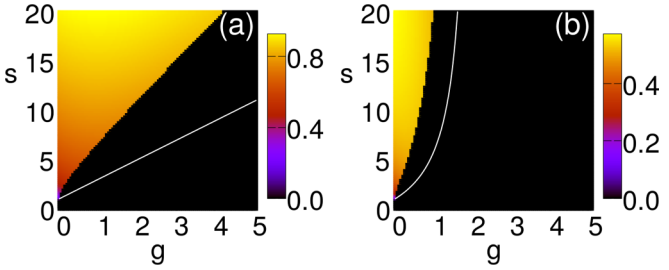

FIG. 2. Bifurcation diagrams in s-g parameter space for two different k values. Plot of s vs g for (a) $k = 0.0$ and (b) $k = 0.5$ in the case of positive chemotaxis. Black regions correspond to the stability of homogeneous steady state and the color represents the wave number of the fastest growing mode of the spatial instability. The white lines represent the onset of instability obtained only from the necessary conditions of instability determined by analytical treatment of linear stability analysis.

To get better insights into how and to what extent growth rate might affect the spatiotemporal organization of a colony, we solve the dispersion relation obtained from model (2). Figure 2 demonstrates the bifurcation diagrams in the s-g parameter plane in the absence and in the presence of the anisotropic production of chemicals, k. These bifurcation diagrams show two different regions: (1) the stable homogeneous region

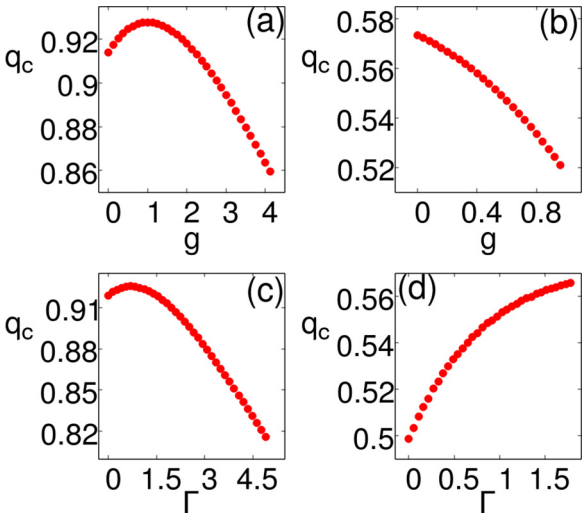

FIG. 3. Dependence of the wave number of the fastest growing mode (q_c) associated with the largest growth rate (maximum eigenvalue) on g and Γ. q_c as a function of g for (a) $k = 0.0$, (b) $k = 0.5$ and plot of q_c vs Γ for (c) $k = 0.0$, (d) $k = 0.5$, obtained from linear stability analysis for $s = 20$. $g = 0.5$ for (c) and (d). All other parameters are the same as given in Table I.

(black) in which the real parts of all the eigenvalues of the dispersion relation are negative and (2) the unstable (stationary with respect to time) region (colored) in which the real part of at least one of the eigenvalues is positive. In the stable region of the bifurcation diagram, the homogeneous steady state remains stable under infinitesimal small perturbation, whereas in the unstable region of parameter space, the homogeneous steady state under infinitesimal perturbation becomes unstable and generates stationary spatial patterns. In the Appendix, we furthermore discuss the conditions of instability and find that no oscillatory instability is possible in the colony under the mechanism of pattern formation by chemoattraction.

We also determine the necessary conditions for instability from the dispersion relation using Routh-Hurwitz criteria (for details, see the Appendix). For $D_p = D_c = \Gamma = 1$, the necessary condition for instability turns out to be $s > (\frac{1+2g}{1-gk})$ (the white lines in Fig. 2) which reveals that gk should be less than 1 for nonzero g and k. If $g = 0$, the instability occurs for $s > 1$ independent of k. With nonzero growth rate, i.e., $g \neq 0$, the minimum value of chemotactic strength s, required to form a stationary pattern increases with g as shown in Fig 2. On the other hand, for a fixed value of s, a very high growth rate of bacteria can remove the spatial instability. This suggests a rapidly growing bacterial colony with high growth rate is less probable to form a spatially patterned colony due to chemotaxis. Moreover, we find that there is an upper limit of g which is independent of s, coming from the condition $gk < 1$, in the case of anisotropic production of chemicals, within which a stationary spatial pattern can emerge.

At this point, we investigate the modulation of the wave number (q_c) of the fastest growing mode ($\partial_{q^2}\lambda = 0$ and $\partial^2_{q^2}\lambda < 0$ at $q = q_c$, where λ is the eigenvalues; for details, see the Appendix) in the presence of the logistic growth dynamics. The wavelength of the pattern is approximately determined by

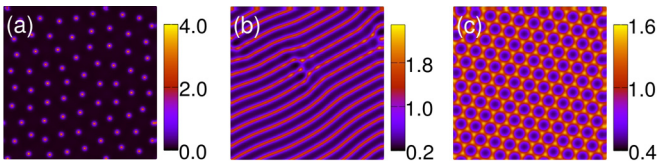

FIG. 4. Snapshots of bacterial density for (a) $g = 0.1$, (b) $g = 1.0$, and (c) $g = 1.5$ for $\Gamma_2 = 0.1$, $s = 10$, and $k = 0$. All other parameters are the same as given in Table I.

$2\pi/q_c$ near the onset of instability [1]. This is only a reasonable prediction, whereas, far from the instability threshold where the interaction caused by the nonlinearities is more complex, the pattern length scale might differ from what we obtain from linearly unstable simpler modes. For isotropic production of chemicals ($k = 0$), q_c first increases slightly with the increase of growth rate up to $g = 1$ and then decreases for higher values of g [see Fig. 3(a)]. However, we observe that q_c decreases with the increase of g for $k \neq 0$ as depicted in Fig. 3(b). Therefore, the wavelength of the patterns will increase with increasing values of g.

We find that the growth rate g in the case of chemoattractive instability in a bacterial colony has twofold effects: (1) it helps to choose a length scale of the patterns by arresting the phase separation and (2) it changes the wavelength of the patterns. Based on their growth environment, bacteria can exhibit a variable growth rate which can thereby control their spatial organization. Depending on the availability of nutrients and favorable environmental conditions, the growth rate of bacteria α can vary and hence can govern the instability conditions.

To further investigate, how the evolution of the polarization vector influences the spatiotemporal instability, we plot the wave number q_c of the pattern as a function of Γ. Γ is controlled by the orientational relaxation of polarization of bacteria and the degradation rate of chemicals. We find that, for $k = 0$, q_c decreases with the increase of Γ, but increases with the increase of Γ for $k \neq 0$ (see Fig. 3). It appears from the necessary conditions of instability as described in the Appendix that increasing Γ requires higher values of s for pattern formation. Bacteria autoaggregate as spots, which is shown in Fig. 1. The arrangement of the spots depends on the parameters (near instability or far from instability) and boundary conditions (periodic or no- flux). We will now turn our attention to the parameter Γ_2, which was not discussed yet since it does not appear in the linear stability analysis of our model (2). We choose $\Gamma_2 = 10$ for all our earlier simulations (unless otherwise mentioned). By decreasing the value of Γ_2, we observe an interesting set of patterns for increasing values of g, such as spots, patterns with continuous formation and breaking of spots, stripes, and inverted spots as shown in Fig. 4. The characteristic length scale of the patterns increases with the decrease of Γ_2. The underlying reason lies in the fact that by decreasing the value of Γ_2, we facilitate the alignment of $\vec{p}$ depending on g (the overall $\vec{\nabla} \cdot \vec{p} = 0$) resulting in different types of patterning unlike the formation of aster and antiaster in the case of higher values of Γ_2.

To this end, motivated by the formation of concentric ring patterns observed in *S. typhimurium* [29,32] colonies, we investigate the pattern development in a growing colony

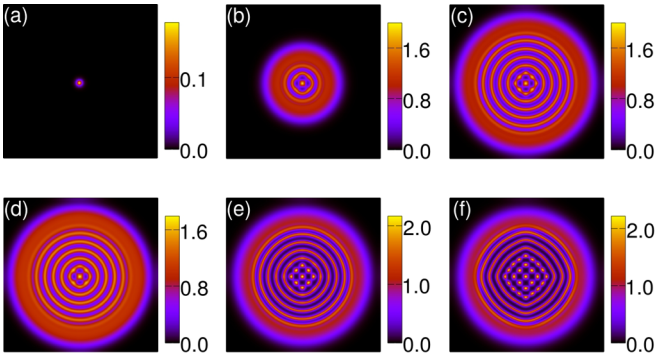

FIG. 5. Time evolution of a droplet of bacterial density from (a) to (c) for $s = 40$. Snapshots of bacterial density for (d) $s = 30$, (e) $s = 80$, and (f) $s = 100$ at a particular time for $k = 0.5$, $g = 0.5$. The dimension of the simulation box is $L = 200$. All other parameters have the same values as given in Table I.

by an initial inoculation of small bacterial droplets at the center of the simulation box. The colony develops concentric rings of bacterial density similar to what is observed in the experiments. Growth helps bacteria to move away from the center of the box but chemoattraction holds them together. The underlying competition between growth dynamics and chemoattraction results in ringlike heterogeneity. Furthermore, we find destabilization of inner rings into small spotlike structures happens with time as shown in Figs. 5(a)–5(c) (see also video 3 in the Supplemental Material [38]). Moreover, we observe that the destabilization of rings occurs faster for large s as shown in Figs. 5(d)–5(f).

B. Emergent patterns due to chemorepulsion

In the case of chemorepulsion ($\chi = -s, s > 0$), bacteria flee away from the self-secreted signaling molecules. The interplay among the chemorepulsive drift, diffusion, and self-secretion of chemicals can potentially generate spatiotemporal patterns giving rise to self-limited cluster sizes even in the absence of growth kinetics similar to what is discussed in [34] in the case of chemorepulsive active colloids. There are two instability mechanisms for the formation of spatial patterns: (1) In the case of "Janus instability" a nonzero value of k (anisotropic production) is important. Bacteria initially goes to the fluctuation-induced local minima of chemical density and due to the asymmetric production of chemicals, a shell of chemorepellent is produced around a cluster of bacterial cells which prevents further recruitment of bacteria resulting in a cluster of self-limited size giving rise to stationary patterns [34]. (2) In the case of "delay-induced" instability, a delayed response of the polarization field creates a feedback loop in which fluctuation of chemical density changes sign which results in oscillatory patterns [34].

To begin our study to understand chemorepulsive pattern formation in the presence of logistic growth, we first draw bifurcation diagrams obtained from the model (2). It can be observed from Fig. 6 that there exist three distinct regimes in the bifurcation diagram: (1) stable homogeneous (black), (2) temporally stable and spatially periodic (colored), and (3) oscillatory and spatially periodic (colored with dots) regions

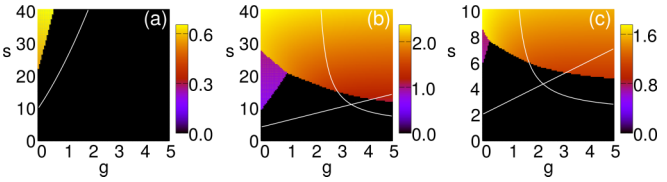

FIG. 6. Bifurcation diagrams in the s-g parameter space for three different k values, (a) $k = 0.0$, (b) $k = 0.5$, and (c) $k = 1.0$ in the case of chemorepulsion. All the other parameters are kept the same as given in Table I. Black regions correspond to the stable state. Color represents the wave number of the fastest growing mode. The white lines in (a) or the union of white lines in (b) and (c) represent the onset of instability coming only from the necessary conditions of instability determined by analytical treatment.

where imaginary parts of the eigenvalues dominate. We see that for the isotropic production of chemicals, i.e., $k = 0$, no stationary pattern formation is possible, which has been discussed in detail in the Appendix. The necessary condition obtained from linear stability analysis for this type of instability is governed by the relation $s > 2g^2 + 12g + 10$ ($k = 0$) as depicted by the white line in Fig. 6(a). For stationary spatial patterns, anisotropic production of chemicals i.e., $k \neq 0$, is a necessity. The necessary condition obtained for this type of instability is governed by $s > \frac{g+2}{k}$ or $s > \frac{2g+1}{kg-1}$ ($k \neq 0$) for $D_p = D_c = \Gamma = 1$ which are only depicted by the white lines in the bifurcation diagrams in Figs. 6(b) and 6(c). A minimum value of chemorepulsive strength $s(>0)$ is required to obtain any spatiotemporal instability in the system and that depends on both the parameters growth rate g and anisotropic production rate k, for fixed values of D_p, D_c, and Γ. This lower limit of s decreases with the increase of g or k in the case of the stationary patterns region. From the bifurcation diagrams as shown in Fig. 6, it is clear that the bacterial colony is unable to exhibit any oscillatory instability for high values of s or g for anisotropic production of chemicals, i.e., $k \neq 0$. With the increase of anisotropic production of chemicals, the oscillatory instability region decreases and

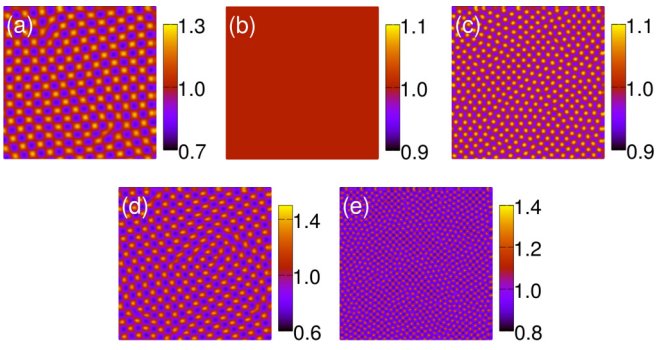

FIG. 7. Shown here are the transitions among spatial patterns obtained by numerically simulating the model under the case of chemorepulsion as a function of growth rate g for fixed chemorepulsive strength s and $k = 0.5$. (i) For the $s = 15$ transition from (a) oscillatory pattern: $g = 0.1$ to (b) homogeneous pattern: $g = 2.0$ to (c) stationary pattern: $g = 4.0$; and (ii) direct transition from (d) oscillatory: $g = 0.4$ to (e) stationary: $g = 1.0$ for $s = 25$. All the other parameters are the same as given in Table I.

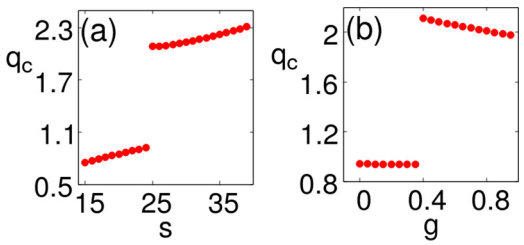

FIG. 8. Dependence of the wave number of the fastest growing mode (q_c) on s and g. For anisotropic production rate $k = 0.5$, (a) q_c vs s at $g = 0.5$ and (b) q_c vs g at $s = 25$ plots, determined from linear stability analysis for the case of chemorepulsion. The other parameters are the same as given in Table I.

ultimately disappears. These observations suggest that in the case of chemorepulsive instabilities, the bacterial growth rate can act as a stabilizing factor to facilitate transitions from an oscillatory to a stationary pattern.

In Fig. 7, we illustrate this transition of patterns with the increase of growth rate g of the bacterial colony by numerically simulating the system described by Eqs. (2). We observe from Figs. 7(a)–7(c), that a transition occurs between oscillatory and stationary states via a homogeneous state for a fixed value of chemorepulsive strength. This two-step transition becomes a one-step transition directly from an oscillatory to a stationary patterned state for a higher value of chemorepulsive strength depending on k as demonstrated in Figs. 7(d) and 7(e). The oscillatory patterns corresponding to Figs. 7(a) and 7(d) are demonstrated in videos 4 and 5 in the Supplemental Material [38].

At this stage, to get a better insight into the pattern transitions, we now investigate how the wavelength of the pattern as determined from the dispersion relation obtained from the linear stability analysis of the system, changes with the variation of chemorepulsive strength and growth rate. In Fig. 8, we plot q_c as a function of s and g. A sudden jump of wavelength with the increase of s or g can be observed, as we move from regions of oscillatory patterns to stationary patterns as shown in Fig. 8. This abrupt change in wavelength also complements the transition among different types of patterns. We also observe ring formation and subsequent breaking of rings into spots in the presence of chemorepulsion while initializing from a small bacterial droplet during colony development.

IV. CONCLUDING REMARKS

Growth and orientational bias are intertwined and regulatory factors in determining the spatiotemporal dynamics of many biological processes such as morphogenesis, cancer metastasis, and biofilm formation. An important feature of those systems is the formation of clusters or multicellular agglomerates of cells to perform certain functions collectively. In bacteria, these agglomerates provide a number of advantages by promoting quorum sensing in biofilm formation, increasing resistance to environmental stresses and emerging collective motions in various circumstances.

In the present work, to understand aggregation of signaling bacteria, we consider an active microbial system of motile cells which show autochemotaxis toward self-secreted signaling molecules and grow by a logistic reaction. Using a spatially extended model in a reaction-drift-diffusion framework, we theoretically studied the interplay of growth, movements, and influence of self-produced signaling chemicals which can capture both the instabilities arising due to chemoattraction and to chemorepulsion. This provides a large set of chemotactic patterns which agrees with experimental observations [12,13]. It turns out that coupling of logistic growth kinetics with chemoattraction arrests the complete phase separation and helps in generating patterns consisting of spots or stripes of well-defined length scale. On the other hand, growth kinetics of bacteria is not the sole factor in arresting the phase separation in the case of chemorepulsion. Due to an anisotropic production of chemicals the clusters are self-limited even in the absence of growth kinetics. However, the wavelength of the patterns undergoes a sudden jump during the transition from oscillatory to stationary states followed by a gradual increase with growth rate. The birth and death dynamics works as an additional mechanism to limit the cluster size along with the self-limiting mechanism arises due to asymmetric production of chemorepellents. By this dual action, the region of instability gets modulated. The oscillatory instability shifts toward stationary instability either via an intermediate stable region or directly with the increase of growth rate. Moreover, we find that the nonlinear cubic saturation of bacterial polarization has a significant effect on the pattern morphology. We come across different types of patterns including stripes, and inverted spots in the case of chemoattractive instability.

The present study illustrates the possible occurrence of different types of natural instabilities as a result of the coupling of orientational bias and growth dynamics in pattern formation in bacteria. In principle, growth kinetics is inherent and system specific. However, in those models also growth dynamics will be a decisive factor for spatiotemporal evolution. Our model might be useful and of considerable interest to investigate similar biological phenomena, e.g., tumor growth and morphogenesis.

ACKNOWLEDGMENTS

We thank Mustansir Barma for discussions. M.M. is supported by graduate fellowship from TIFR Hyderabad. P.G. would like to acknowledge the financial support from Department of Science and Technology, India, INSPIRE Faculty grant (DST/INSPIRE/04/2015/002495).

APPENDIX

Here we perform a detailed linear stability analysis of the system of dimensionless equations:

$$\begin{aligned}
\dot{\rho} &= -\overrightarrow{\nabla}\cdot(\rho\vec{p}) + \nabla^2\rho + g\rho(1-\rho),\\
\dot{\vec{p}} &= -\Gamma\vec{p} + D_p\nabla^2\vec{p} + \chi\overrightarrow{\nabla}c - \Gamma_2|\vec{p}^{\,2}|\vec{p},\\
\dot{c} &= D_c\nabla^2 c + \rho - c + k\overrightarrow{\nabla}\cdot(\rho\vec{p}).
\end{aligned} \tag{A1}$$

We linearize Eqs. (A1) in one dimension about the uniform state $(\rho, p, c) = (\rho_0, 0, \rho_0)$ (where $\rho_0 = 0$ and 1) and

$$\begin{pmatrix} \dot{\delta\rho} \\ \dot{\delta p} \\ \dot{\delta c} \end{pmatrix} = J \begin{pmatrix} \delta\rho \\ \delta p \\ \delta c \end{pmatrix}. \tag{A2}$$

Inserting a plane-wave solution as $(\delta\rho,\delta p,\delta c) = (A_\rho, A_p, A_c)\exp(iqx + \lambda t)$ we get

$$|J - \lambda I| = 0, \tag{A3}$$

where

$$J = \begin{pmatrix} -q^2 + g(1-2\rho_0) & -i\rho_0 q & 0 \\ 0 & -\Gamma - D_p q^2 & i\chi q \\ 1 & i\rho_0 kq & -D_c q^2 - 1 \end{pmatrix}. \tag{A4}$$

δ_ρ, δ_p, and δ_c are the small perturbations around the uniform states. q is the wave number. A_ρ, A_p, and A_c are constants.

The eigenvalue λ can be real or imaginary. For the uniform solution to be stable, all the real parts of λ should be negative. Any positive Re(λ) creates instability in the system resulting in spatial pattern formation. λ represents the growth rate of instability. The wavelength of the pattern is approximately determined by $2\pi/q_c$ near the onset of spatial instability, where q_c is the wave number of the fastest growing unstable mode ($\partial_{q^2}\lambda = 0$ and $\partial^2_{q^2}\lambda < 0$ at $q = q_c$).

In the absence of diffusion, chemotaxis of the uniform state (0,0,0) is unstable but the uniform state (1,0,1) is stable. Therefore, we will consider only the case when $\rho_0 = 1$.

Inserting $\rho_0 = 1$ in Eq. (A5) we get the following dispersion relation:

$$\lambda^3 + a_1\lambda^2 + a_2\lambda + a_3 = 0, \tag{A5}$$

where

$$\begin{aligned} a_1(q^2) &= (D_p + D_c + 1)q^2 + g + \Gamma + 1, \\ a_2(q^2) &= (D_p D_c + D_p + D_c)q^4 + (D_p + D_c\Gamma + 1 + \Gamma + D_c g + D_p g + \chi k)q^2 + \Gamma + g + \Gamma g, \\ a_3(q^2) &= D_p D_c q^6 + (D_p + D_c\Gamma + D_p D_c g + \chi k)q^4 + (\Gamma + D_p g + D_c\Gamma g + \chi k g - \chi)q^2 + \Gamma g. \end{aligned} \tag{A6}$$

Now according to the Routh-Hurwitz criteria [1], the conditions for Re(λ) < 0 are

$$a_1(q^2) > 0, \quad a_3(q^2) > 0 \quad \text{and} \quad a_1(q^2)a_2(q^2) - a_3(q^2) > 0, \tag{A7}$$

where

$$\begin{aligned} a_1(q^2)a_2(q^2) - a_3(q^2) = {} & (D_p + D_c)(D_p + 1)(D_c + 1)q^6 + [D_c^2 g + D_c^2\Gamma + D_p^2 g + D_p^2 + 2D_p D_c g + 2D_p D_c\Gamma \\ & + 2D_p D_c + 2D_c g + 2D_c\Gamma + 2D_p g + 2D_p\Gamma + 2D_p + 2D_c + \Gamma + 1 + \chi k(D_p + D_c)]q^4 \\ & + [D_c g^2 + D_c\Gamma^2 + 2D_c g\Gamma + 2D_c g + 2D_c\Gamma + D_p g^2 + 2D_p g\Gamma + 2D_p g + 2D_p\Gamma + D_p + 2g\Gamma + 2g \\ & + (\Gamma + 1)^2 + \chi + \chi k(\Gamma + 1)]q^2 + (\Gamma + g + 1)(\Gamma + g + \Gamma g) - \Gamma g. \end{aligned} \tag{A8}$$

The conditions for instability are

$$a_1(0) > 0, \quad a_3(0) > 0, \quad a_1(0)a_2(0) - a_3(0) > 0$$

and at least one of $a_1(q^2), a_3(q^2), a_1(q^2)a_2(q^2) - a_3(q^2) < 0$ for some nonzero q^2.

$a_1(q^2)$ is always greater than zero [see (A6)]. a_3 and $a_1a_2 - a_3$ both tend to ∞ when $q^2 \to \infty$ provided that D_p or $D_c \neq 0$. Therefore, a finite range of q can be driven unstable. We can estimate the wavelength of the emerging pattern.

a_3 and $a_1a_2 - a_3$ both are cubic functions of q^2 as $Y(q^2) = A(q^2)^3 + B(q^2)^2 + C(q^2) + D$ with $A, D > 0$. They both are positive at $q^2 = 0$ and $q^2 \to \infty$. For instability one of them should be negative. The minimum turning point can be obtained by $\partial_{q^2}Y = 0$ and $\partial^2_{q^2}Y > 0$. We get minimum of Y at

$$q_*^2 = \frac{-B + \sqrt{B^2 - 3AC}}{3A}. \tag{A9}$$

q_*^2 is real and positive if $B < 0$ or $C < 0$ and $B^2 > 3AC$. And we get a complicated condition from $Y(q_*^2) < 0$.

The conditions are too complicated to handle analytically. From now on, we only consider the conditions $B < 0$ or $C < 0$. These are the necessary conditions for instability.

The instability can be of two types: the stationary instability (where λ is real and positive) and oscillatory instability (where the imaginary part of λ dominates). By considering λ as an imaginary quantity, we can find the conditions on a_2, a_3, and $a_1a_2 - a_3$ (see Table 3 of [39]) to determine the nature of emerging patterns, whether spatial or spatiotemporal.

At the threshold of instability, the minimum turning point of a_3 (A9) matches with q_c. So, at this point we can determine the wavelength pattern which is $\approx 2\pi/q_*$ where $q_* = \frac{-(D_p + D_c\Gamma + D_p D_c g + \chi k)}{3D_p D_c} + \frac{\sqrt{(D_p + D_c\Gamma + D_p D_c g + \chi k)^2 - 3D_p D_c(\Gamma + D_p g + D_c\Gamma g + \chi k g - \chi)}}{3D_p D_c}$. We also solve Eq. (A5) numerically to find the bifurcation diagrams in any two parameters space by choosing other parameters constant and find the wave number (or wavelength) of emerging patterns (see main text).

Chemoattraction. For chemoattraction $\chi = s$, where $s > 0$. Therefore, $a_1a_2 - a_3 > 0$. The instability condition can only be obtained by a_3. So, the necessary condition for instability is $(\Gamma + D_p g + D_c\Gamma g + skg - s) < 0$.

For the special case, $\Gamma = D_p = D_c = 1$, the condition becomes $s > \frac{1+2g}{1-kg}$, where $gk < 1$, which sets the upper limit

of g at a fixed k ($\neq 0$) or upper limit of k at a fixed g ($\neq 0$) independent of s.

Here, in the instability region, $a_3 < 0$ and $a_1a_2 - a_3 > 0$. According to Table 3 of [39], to get an oscillatory pattern, a_2 must be negative. But, in our case a_2 is positive. So, for chemoattraction no oscillatory pattern is possible; we only get stationary spatial patterns for nonzero g.

Chemorepulsion. For chemorepulsion we choose $\chi = -s$, where $s > 0$. The necessary instability conditions can be found from a_3 and $a_1a_2 - a_3$. Both can be negative. So, the conditions become

a_3:

$$(D_p + D_c\Gamma + D_pD_cg - sk) < 0$$

or

$$(\Gamma + D_pg + D_c\Gamma g - skg + s) < 0. \tag{A10}$$

$a_1a_2 - a_3$:

$$\begin{aligned}&[D_c^2g + D_c^2\Gamma + D_p^2g + D^2p + 2D_pD_cg + 2D_pD_c\Gamma\\ &+ 2D_pD_c + 2D_cg + 2D_c\Gamma + 2D_pg + 2D_p\Gamma\\ &+ 2D_p + 2D_c + \Gamma + 1 - sk(D_p + D_c)] < 0\end{aligned}$$

or

$$\begin{aligned}&[D_cg^2 + D_c\Gamma^2 + 2D_cg\Gamma + 2D_cg + 2D_c\Gamma + D_pg^2\\ &+ 2D_pg\Gamma + 2D_pg + 2D_p\Gamma + D_p + 2g\Gamma + 2g\\ &+ (\Gamma + 1)^2 - s - sk(\Gamma + 1)] < 0.\end{aligned} \tag{A11}$$

We can obtain these necessary conditions according to the value of k.

Case 1 ($k = 0$). For this case, $a_3 > 0$. The condition of instability can only be obtained from $a_1a_2 - a_3$. For $\Gamma = D_p = D_c = 1$, the condition becomes

$$s > 2g^2 + 12g + 10. \tag{A12}$$

Here, in the instability region, $a_2 > 0$, $a_3 > 0$, and $a_1a_2 - a_3 < 0$. So, no stationary instability is possible; we can only get spatiotemporal patterns (see Table 3 of [39]).

Case 2 ($k \neq 0$). For $\Gamma = D_p = D_c = 1$, the conditions become

a_3:

$$s > \frac{g+2}{k} \quad \text{or} \quad s > \frac{2g+1}{kg-1}. \tag{A13}$$

$a_1a_2 - a_3$:

$$s > \frac{4g+8}{k} \quad \text{or} \quad s > \frac{2g^2+12g+10}{2k+1}. \tag{A14}$$

The conditions in (A14) are a subset of the conditions in (A13). So, we can consider the conditions in (A13) as necessary conditions of instability. In this case, both stationary and oscillatory instabilities are possible, although we cannot differentiate between stationary and oscillatory instabilities from these conditions.

We also calculate the length scale of the patterns directly from the numerical solution of Eqs. (A1) using the relation

$$L(t) = \frac{\sum_{\vec{q}} |a(\vec{q},t)|^2}{\sum_{\vec{q}} q|a(\vec{q},t)|^2}, \tag{A15}$$

where $a(\vec{q},t)$ is the Fourier amplitude of $\delta\rho(\vec{r},t) = \rho(\vec{r},t) - \overline{\rho(t)}$ and $\overline{\rho(t)} = \frac{1}{N^2}\sum_{\vec{r}} \rho(\vec{r},t)$ for a $N \times N$ square grid. The sum in (A15) is dominated by $q = q_c$ at which $|a(\vec{q},t)|$ has a sharp maxima.

[1] J. D. Murray, *Mathematical Biology. II: Spatial Models and Biomedical Applications*, 3rd ed. (Springer, New York, 2003), Vol. 18.

[2] L. Hall-Stoodley, J. W. Costerton, and P. Stoodley, Nat. Rev. Microbiol. **2**, 95 (2004).

[3] T. Tolker-Nielsen and S. Molin, Microb. Ecol. **40**, 75 (2000).

[4] E. Ben-Jacob, I. Cohen, and H. Levine, Adv. Phys. **49**, 395 (2000).

[5] M. C. Marchetti, J. F. Joanny, S. Ramaswamy, T. B. Liverpool, J. Prost, M. Rao, and R. A. Simha, Rev. Mod. Phys. **85**, 1143 (2013).

[6] H.-C. Flemming and J. Wingender, Nat. Rev. Microbiol. **8**, 623 (2010).

[7] R. M. Donlan, Emerg. Infect. Dis. **8**, 881 (2002).

[8] G. E. Dilanji, M. Teplitski, and S. J. Hagen, Proc. R. Soc. London, Ser. B **281**, 20132575 (2014).

[9] P. Ghosh, J. Mondal, E. Ben-Jacob, and H. Levine, Proc. Natl. Acad. Sci. USA **112**, E2166 (2015).

[10] P. Ghosh and H. Levine, Phys. Rev. E **96**, 052404 (2017).

[11] C. M. Waters and B. L. Bassler, Annu. Rev. Cell Dev. Biol. **21**, 319 (2005).

[12] L. Laganenka, R. Colin, and V. Sourjik, Nat. Commun. **7**, 12984 (2016).

[13] C. Liu, X. Fu, L. Liu, X. Ren, C. K. Chau, S. Li, L. Xiang, H. Zeng, G. Chen, L.-H. Tang *et al.*, Science **334**, 238 (2011).

[14] M. Asally, M. Kittisopikul, P. Rué, Y. Du, Z. Hu, T. Çağatay, A. B. Robinson, H. Lu, J. Garcia-Ojalvo, and G. M. Süel, Proc. Natl. Acad. Sci. USA **109**, 18891 (2012).

[15] P. Ghosh, E. Ben-Jacob, and H. Levine, Phys. Biol. **10**, 066006 (2013).

[16] M. E. Cates, D. Marenduzzo, I. Pagonabarraga, and J. Tailleur, Proc. Natl. Acad. Sci. USA **107**, 11715 (2010).

[17] X. Yang, D. Marenduzzo, and M. C. Marchetti, Phys. Rev. E **89**, 012711 (2014).

[18] M. E. Cates and J. Tailleur, Annu. Rev. Condens. Matter Phys. **6**, 219 (2015).

[19] S. Payne, B. Li, Y. Cao, D. Schaeffer, M. D. Ryser, and L. You, Mol. Syst. Biol. **9**, 697 (2013).

[20] G. E. Dilanji, J. B. Langebrake, P. De Leenheer, and S. J. Hagen, J. Am. Chem. Soc. **134**, 5618 (2012).

[21] J. B. Langebrake, G. E. Dilanji, S. J. Hagen, and P. D. Leenheer, J. Theor. Biol. **363**, 53 (2014).

[22] T. Hillen and K. J. Painter, J. Math. Biol. **58**, 183 (2008).

[23] T. Curk, D. Marenduzzo, and J. Dobnikar, PLoS One **8**, e74878 (2013).

[24] R. Tyson, S. R. Lubkin, and J. D. Murray, Proc. R. Soc. London, Ser. B **266**, 299 (1999).
[25] R. Tyson, S. R. Lubkin, and J. D. Murray, J. Math. Biol. **38**, 359 (1999).
[26] Y. Hong, N. M. K. Blackman, N. D. Kopp, A. Sen, and D. Velegol, Phys. Rev. Lett. **99**, 178103 (2007).
[27] S. Saha, R. Golestanian, and S. Ramaswamy, Phys. Rev. E **89**, 062316 (2014).
[28] L. Tsimring, H. Levine, I. Aranson, E. Ben-Jacob, I. Cohen, O. Shochet, and W. N. Reynolds, Phys. Rev. Lett. **75**, 1859 (1995).
[29] M. P. Brenner, L. S. Levitov, and E. O. Budrene, Biophys. J. **74**, 1677 (1998).
[30] J. K. Anderson, J. Y. Huang, C. Wreden, E. G. Sweeney, J. Goers, S. J. Remington, and K. Guillemin, mBio **6**, e00379 (2015).
[31] E. O. Budrene and H. C. Berg, Nature (London) **349**, 630 (1991).
[32] D. E. Woodward, R. Tyson, M. R. Myerscough, J. D. Murray, E. O. Budrene, and H. C. Berg, Biophys. J. **68**, 2181 (1995).
[33] E. F. Keller and L. A. Segel, J. Theor. Biol. **30**, 225 (1971).
[34] B. Liebchen, D. Marenduzzo, I. Pagonabarraga, and M. E. Cates, Phys. Rev. Lett. **115**, 258301 (2015).
[35] B. Liebchen, D. Marenduzzo, and M. E. Cates, Phys. Rev. Lett. **118**, 268001 (2017).
[36] B. Liebchen, M. E. Cates, and D. Marenduzzo, Soft Matter **12**, 7259 (2016).
[37] T. Le Goff, B. Liebchen, and D. Marenduzzo, Phys. Rev. Lett. **117**, 238002 (2016).
[38] See Supplemental Material at http://link.aps.org/supplemental/10.1103/PhysRevE.97.012413 for the corresponding video files demonstrating the different types of pattern formation as mentioned in the main text.
[39] K. A. J. White and C. A. Gilligan, Philos. Trans. R. Soc., B **353**, 543 (1998).